THE ASTRONOMICAL JOURNAL, 121:740–752, 2001 February

WARM MOLECULAR GAS IN DWARF STARBURST GALAXIES: CO(3–2) OBSERVATIONS

DAVID S. MEIER, JEAN L. TURNER, AND LUCIAN P. CROSTHWAITE
Department of Physics and Astronomy, University of California, Los Angeles, CA90095-1562; meierd@astro.ucla.edu, turner@astro.ucla.edu, lucian@astro.ucla.edu

AND

SARA C. BECK
Department of Physics and Astronomy, Tel Aviv University, 69978 Ramat Aviv, Israel; sara@wise.tau.ac.il
Received 1999 August 23; accepted 2000 November 6

ABSTRACT

Eight dwarf starburst galaxies have been observed with the Caltech Submillimeter Observatory telescope in the CO $J = 3$–2 transition. The galaxies observed are He 2-10, NGC 5253, 1569, and 3077, Haro 2, Haro 3, II Zw 40, and Mrk 86; all but the last two are detected. The central regions of He 2-10 and NGC 5253 were mapped and a CO(2–1) spectrum of NGC 5253 was obtained. The error-weighted mean CO(3–2)/CO(1–0) ratio of the detected galaxies is 0.60 ± 0.06, which is virtually identical to that found for starbursts in the nuclei of nearby spirals and suggests that the molecular gas is optically thick, warm ($T_k > 20$ K), and moderately dense ($n_{H_2} \sim 10^3$–10^4 cm^{-3}). The CO(3–2)/CO(1–0) ratio peaks at or close to the starburst in all cases. CO emission does not appear to be optically thin in these dwarfs, despite the low metallicity and intense radiation fields, probably because for CO to exist in detectable amounts it must be self-shielding and hence optically thick. Physical properties of the molecular clouds in these dwarf starbursts appear to be essentially the same as those in nearby spiral nuclei, with the possible exception that CO is more confined to the cloud cores.

Key words: galaxies: dwarf — galaxies: ISM — galaxies: nuclei — galaxies: starburst — radio emission lines

1. INTRODUCTION

Dwarf galaxies differ in many characteristics from large star-forming spirals. Typically they are much smaller ($\lesssim 3$ kpc), have lower rotation velocities ($\lesssim 30$ km s^{-1}), generally warmer interstellar media ($T_d > 30$ K), and solid body rotation, lack density waves, and present less complicated star-forming environments than spiral galaxies (e.g., Hodge 1971; Gallagher & Hunter 1984; Thronson & Telesco 1986). Also, dwarf galaxies are different in composition, appearing to have relatively high H I and dark matter fractions (Thuan & Martin 1981), relatively little dust, and lower metallicities. The molecular content in dwarf galaxies is particularly difficult to study, since CO(1–0) is usually quite weak because of the low metallicities and is therefore probably not a good tracer of H_2 (Israel et al. 1986; Verter & Hodge 1995; Wilson 1995).

The relatively weak CO(1–0) emission in dwarf galaxies leads us to search for a stronger line with which to study molecular gas. The $J = 3$–2 transition of CO may be more easily detected in dwarf starbursts since it is relatively easily excited in warm gas ($E/k = 33.2$ K). Because of its higher characteristic temperature and critical density ($n_{cr} \sim 2 \times 10^3$ cm^{-3}), the CO(3–2) transition may be more sensitive to warm, dense gas directly involved in the starburst. It also has a greater optical depth than the CO(1–0), which can make it easier to detect if CO(1–0) is optically thin.

A sample of nearby dwarf starbursts has been observed in the CO(3–2) transition with the Caltech Submillimeter Observatory. Among the questions addressed are the following: Do molecular clouds in dwarf galaxies have different physical properties than their higher metallicity counterparts? Is the CO(1–0) line weak in dwarf galaxies because it is optically thin? Is the CO conversion factor in dwarf starbursts different from large spirals because of these physical conditions?

1.1. *Galaxy Sample*

A sample of eight nearby ($\lesssim 20$ Mpc) dwarf starburst galaxies was observed. The galaxies are He 2-10, NGC 5253, 1569, and 3077, Haro 2, Haro 3, II Zw 40, and Mrk 86. The sample is heterogeneous and illustrative but not complete or unbiased. Galaxies were selected based on the following criteria: they have been previously observed and detected in either the CO(1–0) or CO(2–1) transition (Wiklind & Henkel 1989; Becker, Schilke, & Henkel 1989; Sage et al. 1992; Baas, Israel, & Koornneef 1994; Greve et al. 1996), have IRAS 100 μm fluxes greater than 5 Jy (Thronson & Telesco 1986; Melisse & Israel 1994), are fainter than $M_B > -18.5$, and have undergone a recent burst of intense star formation. All the galaxies except NGC 3077 and Mrk 86 have Wolf-Rayet (WR) emission features (e.g., Conti 1991; Steel et al. 1996; Gonzalez Delgado et al. 1997; Schaerer, Contini, & Pindao 1999). Some of these galaxies contain super–star clusters (He 2-10, NGC 5253, NGC 1569, and Haro 3; Conti & Vacca 1994; Meurer et al. 1995; Arp & Sandage 1985; Steel et al. 1996). A number of these dwarfs show signs of interaction (He 2-10, NGC 5253, 1569, and 3077, and II Zw 40). The properties of the galaxies in the sample are shown in Table 1.

2. OBSERVATIONS

We observed the ^{12}CO(3–2) line (345.796 GHz) toward the galaxies He 2-10, NGC 5253, and II Zw 40 on 1997 February 24 and February 25, and the remaining five galaxies on 1999 January 14 and January 15, using the 10.4 m Caltech Submillimeter Observatory (CSO). The beam size of the CSO at 345 GHz is 22″. Facility SIS receivers were used, together with a 1024 channel 500 MHz AOS spectrometer. System temperatures ranged from 600 to 1100 K for the 1997 data and 700 to 900 K in 1999 ($\tau_{225} \simeq 0.08$–0.15). Pointing was checked using IRC +10216, α Orionis (1997

TABLE 1

THE GALAXY SAMPLE

Galaxy	R.A. (B1950)	Decl. (B1950)	Dist. (Mpc)	$-M_B$	IRAS 60/100 μm (Jy)	T_D[a] (K)	log L_{FIR} ($L_\odot$)	M_D[b] ($M_\odot$)	log $M_{H\,I}$ ($M_\odot$)	[O/H]	References
He 2-10	08 34 07.3	−26 14 05.9	9.0	17.4	24.0/26.4	43	9.43	5.47	8.53	8.93	1, 9, 10, 11
NGC 5253.....	13 37 05.8	−31 23 19.0	4.1	17.2	30.9/29.0	46	8.98	4.73	8.3	8.10	12, 15, 19, 22, 23
NGC 1569.....	04 26 02.0	64 44 31.0	2.2	16.9	46.3/50.7	43	8.65	4.52	7.93	8.19	5, 6, 7, 13, 22
NGC 3077.....	09 59 20.0	68 58 30.0	3.25	16.1	14.7/26.9	34	8.70	4.99	9.00	9.02	2, 4, 16, 17, 21
Haro 2	10 29 22.7	54 39 24.0	20.3	18.4	4.7/5.3	42	9.60	5.51	8.68	8.4	1, 14, 18, 22
Haro 3	10 42 16.5	56 13 23.0	13.7	17.5	5.1/6.4	41	9.30	5.16	8.79	8.4	8, 18, 20, 22
II Zw 40	05 53 04.9	03 23 06.0	9.2	16.2	6.5/5.7	48	9.04	4.66	8.3	8.15	3, 8, 18, 22
Mrk 86	08 09 42.8	46 08 33.0	6.3	16.6	3.2/6.3	33	8.45	5.00	8.28	8.05[c]	8, 18, 22

NOTE.—Units of right ascension are hours, minutes, and seconds, and units of declination are degrees, arcminutes, and arcseconds.

[a] Using $R(60/100) = 0.6^{-4}(e^{136/T_D} - 1)/(e^{226/T_D} - 1)$,Thronson & Telesco 1986.

[b] Using $M_D = 5D^2F_{Jy}(e^{144/T_D} - 1)$, Thronson & Telesco 1986.

[c] Extrapolated from the absolute magnitude based on the relationship of Skillman, Kennicutt, & Hodge 1989.

REFERENCES.—(1) Baas et al. 1994; (2) Cottrell 1976; (3) Garnett 1990; (4) Heckman 1980; (5) Israel 1988; (6) Israel & de Bruyn 1988; (7) Israel & van Driel 1990; (8) Klein, Weiland, & Brinks 1991; (9) Kobulnicky et al. 1995; (10) Kobulnicky & Johnston 1999; (11) Kobulnicky, Kennicutt, & Pizagno 1999; (12) Kobulnicky & Skillman 1995; (13) Kobulnicky & Skillman 1997; (14) Kunth & Jobert 1985; (15) Marconi, Matteucci, & Tosi 1994; (16) Melisse & Israel 1994; (17) Niklas et al. 1995; (18) Sage et al. 1992; (19) Sandage 1994; (20) Steele et al. 1996; (21) Tammann & Sandage 1968; (22) Thronson & Telesco 1986; (23) Turner, Ho, & Beck 1998.

TABLE 2

RESULTS

$(\Delta\alpha, \Delta\delta)$ (arcsec)	V_{LSR} (km s^{-1})	ΔV (km s^{-1})	T_{mb} (K)	I_{CO} (K km s^{-1})
He 2-10,3–2:				
(0,0)	849 ± 1.0	56.6 ± 2.3	0.27 ± 0.018	16.6 ± 0.6
(0,−10)	846 ± 1.6	63.8 ± 3.7	0.20 ± 0.018	13.3 ± 0.7
(−10,0)	854 ± 1.5	58.8 ± 3.6	0.19 ± 0.02	11.9 ± 0.6
(0, 1).....	850 ± 2.0	63.4 ± 4.8	0.15 ± 0.022	10.3 ± 0.7
(10, 0	846 ± 1.4	50.0 ± 3.4	0.24 ± 0.022	12.6 ± 0.7
(10, 10)	849 ± 3.0	61.7 ± 7.0	0.12 ± 0.016	7.77 ± 0.8
(10, −10)	833 ± 1.8	37.2 ± 4.4	0.19 ± 0.023	7.47 ± 0.7
(10, −20)	872 ± 14.4	140 ± 25	0.047 ± 0.024	7.00 ± 1.4
(20, 10)	826 ± 3.3	22.5 ± 7.1	0.090 ± 0.022	2.16 ± 0.6
(0, −20).....	845 ± 5.6	33.0 ± 4.4	0.072 ± 0.030	2.53 ± 0.8
(−10, −10).....	851 ± 2.3	59.7 ± 6.5	0.142 ± 0.020	9.06 ± 0.8
(20, 0)	...	...	≤0.053	...
(−10, 10)	855 ± 3.0	73.7 ± 7.7	0.094 ± 0.019	7.4 ± 0.6
(20, −10)	825 ± 3.9	26.7 ± 10.8	0.103 ± 0.022	2.91 ± 0.7
NGC 5253, 3–2:				
(0, 0).....	421 ± 4.2	45.4 ± 8.7	0.070 ± 0.021	3.39 ± 0.6
(10, −10)	...	...	≤0.073	...
(20, 20)	...	...	≤0.069	...
(15, 25)	...	...	≤0.075	...
NGC 5253, 2–1:				
(0, 0).....	407 ± 2.9	71.6 ± 9.0	0.034 ± 0.006	2.58 ± 0.3
NGC 1569, 3–2:				
(0, 0).....	−68.4 ± 2.0	32.3 ± 4.0	0.063 ± 0.01	2.2 ± 0.3
NGC 3077, 3–2:				
(0, 0).....	7.80 ± 2.9	50.9 ± 7.0	0.10 ± 0.02	5.5 ± 0.6
Haro 2, 3–2:				
(0, 0).....	1422 ± 4.6	68.8 ± 9.8	0.032 ± 0.01	2.3 ± 0.3
Haro 3, 3–2:				
(0, 0).....	951 ± 4.6	52.6 ± 14	0.034 ± 0.01	1.9 ± 0.4
II Zw 40, 3–2:				
(0, 0).....	...	...	≤0.021	≤0.9
Mrk 86, 3–2:				
(0, 0).....	...	...	≤0.033	≤1.8

NOTE.—Offsets are in arcseconds from the central position listed in Table 1. Errors are 1 σ from a Gaussian fit, based only on the uncertainty in the spectrum. The noise in the Gaussian fit for Haro 2 is worse than the actual noise in the spectrum, implying it is not Gaussian- shaped (see text). For nondetections 3 σ limits are quoted. The uncertainties in absolute calibration were not included.

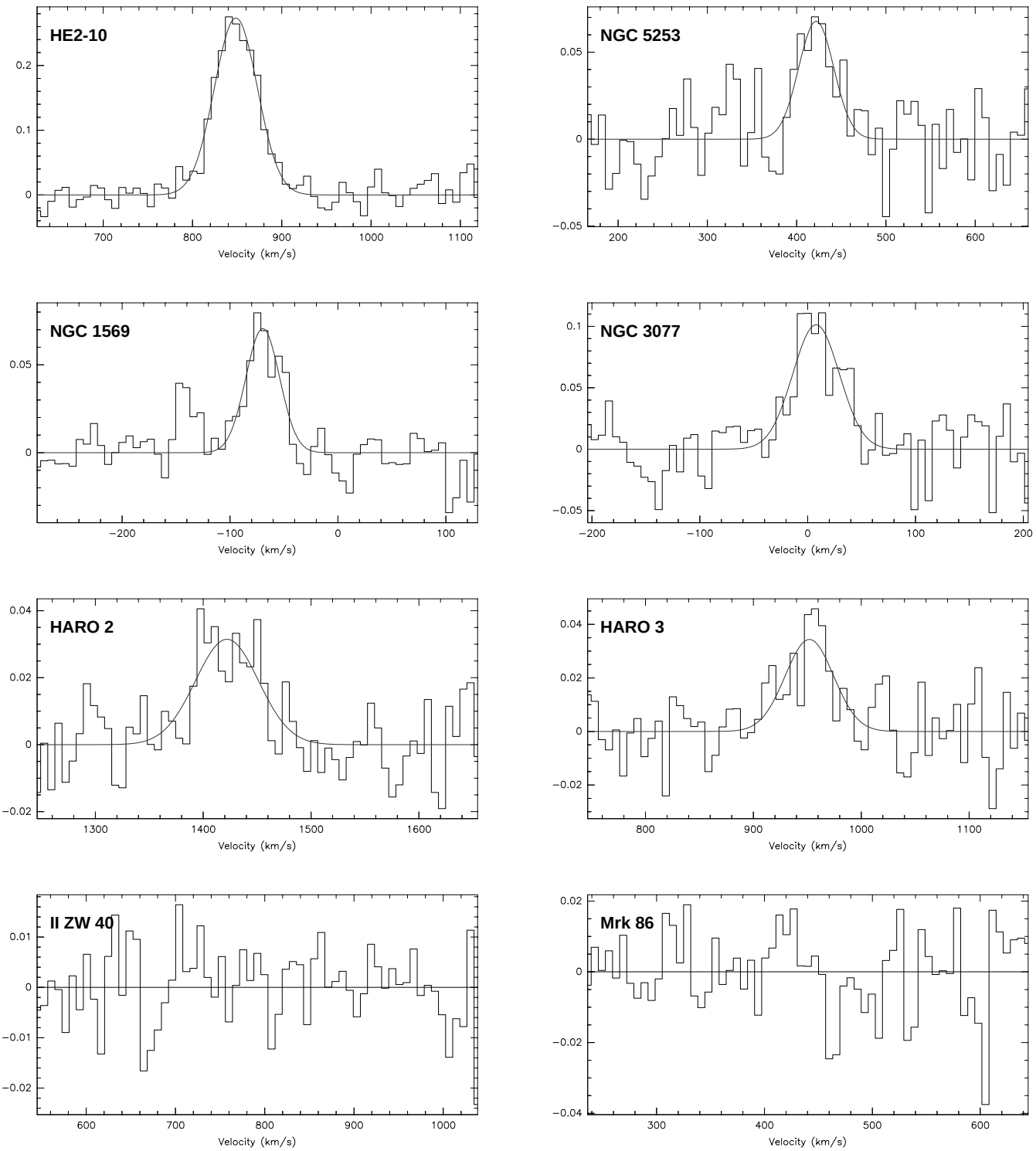

FIG. 1.—CO(3–2) spectra of the eight galaxies, showing the main-beam temperature in kelvins (*vertical axis*) and the velocity (LSR) in kilometers per second (*horizontal axis*). The line represents the least-squares fitted Gaussian.

observations), Saturn, and Mars (1999). Absolute pointing uncertainty was $\leq 6''$ and was repeatable to $\leq 3''$–$4''$. Reported temperatures are main-beam temperatures, the brightness temperature a source would have if it uniformly filled the main beam and was zero elsewhere. The main-beam efficiencies used to convert the antenna temperature to the main-beam temperature were determined from observations of Mars and found to be $\eta_{\rm mb} = 0.6$ (1997) and 0.62 (1999). Since no published CO(2–1) spectrum exists for NGC 5253, G. Serabyn kindly obtained one for us on 1997 May 28. At 230 GHz, the CSO beam size is 30″, and $\eta_{\rm mb} = 0.65$, as determined from observations of Mars. System temperatures for this spectrum are $\sim$400 K. Second-order or lower polynomials were removed from each scan to give flat baselines. The scans were then averaged, using $1/T_{\rm sys}^2$ weights. The spectra were Hanning smoothed to a resolution of 7.8 km s^{-1} (1997) and 6.6 km s^{-1} (1999). Reduction of the spectra was done in CLASS. For He 2-10,

the maps were made and analyzed using the NRAO Astronomical Image Processing System package.

2.1. CO(3–2) *Spectra*

CO(3–2) spectra of the central positions of each of the galaxies are displayed in Figure 1. We detected CO(3–2) in all the galaxies except Mrk 86 and II Zw 40. Line intensities, uncertainties, and Gaussian fits are tabulated in Table 2. For some of the spectra Gaussians may not represent the true line profile, but given the weakness of the signal fitting anything more complicated is unwarranted. The details of each galaxy are discussed in § 6.

In general CO(3–2) is very weak ($T_{mb} \sim 0.05$ K) over our projected beam sizes of 0.25–2 kpc. This is not surprising; dwarf galaxies are known to be weak in the other low J CO lines (Young, Gallagher, & Hunter 1984; Israel 1986; Tacconi & Young 1987; Arnault et al. 1988; Sage et al. 1992). However, CO(3–2) is strong relative to CO(1–0) and CO(2–1). Only one of the six detected galaxies has a CO(3–2)/CO(1–0) ratio as low as 0.4, which is typical of the Galactic disk. Comparing the CO(3–2)/CO(1–0) line ratio with the CO(2–1)/CO(1–0) line ratio, we find that galaxies with high 2–1/1–0 ratios tend to have high 3–2/1–0 ratios. There is one notable exception, II Zw 40. II Zw 40 has a high CO(2–1)/CO(1–0) ratio (Sage et al. 1992), but its CO(3–2)/CO(1–0) ratio is ≤ 0.43 (1 σ).

3. LINE RATIOS: PHYSICAL PROPERTIES OF THE MOLECULAR GAS

CO line ratios can be used to investigate molecular gas properties in these starbursts. CO(3–2)/CO(1–0) ratios are more sensitive to gas temperature than CO(2–1)/CO(1–0) ratios because of the larger separation in J. Thanks to the fortuitous matching of the CO(1–0) beam at the IRAM 30 m ($\sim 21''$) telescope and the CO(3–2) beam at the CSO ($\sim 22''$), CO(3–2)/CO(1–0) line ratios can be estimated without assumptions about source structure. Only the two southern galaxies, He 2-10 and NGC 5253, lack IRAM CO(1–0) spectra. For these two galaxies, the source has been mapped at CO(3–2) or with an interferometer at CO(2–1) or both (Meier & Turner 1998).

Along with the CO(3–2)/CO(1–0) line ratios, Table 3 includes CO(2–1)/CO(1–0) line ratios. The CO(2–1) observations do not have matching beams. Therefore Table 3 indicates what ratio would be predicted in the point-source limit (source much smaller than either beam) and in the uniform filling limit (source much larger than both beams). These line ratios are calculated using

$$R_{ij} = \frac{I_{21}}{I_{10}} \frac{\Omega_s + {}^{21}\Omega_B}{\Omega_s + {}^{10}\Omega_B},$$

where Ω_s, ${}^{21}\Omega_B$, and ${}^{10}\Omega_B$ are the source solid angle and the solid angle of the beams at the respective transitions and I_{21} and I_{10} are their observed line intensities (e.g., Rohlfs & Wilson 1996, p 362). For sources that have been mapped a deconvolved ratio based on the measured Ω_s is also included. In all cases with the possible exception of CO(2–1)/CO(1–0) in NGC 1569 the uniform filling ratios are unrealistically high, implying that the sources are small. This is consistent with the low filling factor found for these galaxies (§ 3.1)

The CO(3–2)/CO(1–0) ratios in the dwarf starbursts range from 0.37 to 1.1. The error-weighted mean CO(3–2)/CO(1–0) line ratio for the sample is 0.6 ± 0.06. (We have estimated the uncertainty in the line ratio as the noise error in each spectrum added in quadrature with 20% absolute calibration uncertainties.) This error-weighted ratio is identical within the uncertainties to that found for a sample of nondwarf starburst nuclei (0.64; Devereux et al. 1994) and for nearby luminous IR galaxies (~ 0.7; Mauersberger et al. 1999). The value is higher than the value obtained for Galactic giant molecular clouds, 0.4, and closer to the value obtained for star-forming cores in the Galaxy (0.6; Sanders et al. 1993).

TABLE 3

CO LINE RATIOS

Galaxy[a]	3–2/1–0	3–2/2–1	2–1/1–0
He 2-10:			
PS	0.50 ± 0.1	0.87 ± 0.2	0.48 ± 0.07
(0,0), U.....	1.7 ± 0.3	0.96 ± 0.2	1.73 0.3
D	*0.61 ± 0.1	0.96 ± 0.2	*0.59 ± 0.1
NGC 5253:			
PS	0.65 ± 0.2	0.70 ± 0.2	0.93 ± 0.2
(0,0), U	2.6 ± 0.7	1.3 ± 0.4	2.0 ± 0.4
D	*0.70 ± 0.2	0.73 ± 0.2	*0.96 ± 0.25
NGC 1569:			
PS	*1.00 ± 0.2	2.5 ± 0.6	0.42 ± 0.1
U	1.10 ± 0.2	0.88 ± 0.2	1.10 ± 0.2
D	...	...	*1.10 ± 0.2
NGC 3077:			
PS	*0.95 ± 0.2	2.1 ± 0.7	0.55 ± 0.1
U	1.04 ± 0.25	0.83 ± 0.2	1.2 ± 0.3
D	...	...	*0.82 ± 0.2
Haro 2:			
PS	*0.34 ± 0.1	1.1 ± 0.2	*0.31 ± 0.10
U	0.37 ± 0.1	0.96 ± 0.2	1.0 ± 0.1
Haro 3:			
PS	*0.89 ± 0.3	1.7 ± 0.5	*0.50 ± 0.09
U	0.97 ± 0.3	0.57 ± 0.2	1.7 ± 0.3
II Zw 40:			
PS	≤ 0.39	...	0.58 ± 0.16
U	≤ 0.43	≤ 0.24	1.78 0.32
Mrk 86:			
PS	≤ 0.41	...	0.31 ± 0.11
U	≤ 0.45	≤ 0.52	1.0 ± 0.36

NOTE.—See the text for the description of the method for finding each ratio and the estimation of the errors. The slight difference between the IRAM 30 m (1–0) beam and the CSO (3–2) beam has been accounted for in the calculations of the ratios. An asterisk denotes which value of the line ratio is used in the LVG modeling. All line ratios are based on a 22″ beam size except He 2-10 and NGC 5253, which are based on a 40″ beam size. The data for the 2–1 and 1–0 emission come from Baas et al. 1994 (He 2-10), Wiklind & Henkel 1989 and this paper (NGC 5253), Greve et al. 1996 (NGC 1569), Becker et al. 1989 (NGC 3077), and Sage et al. 1992 (others).

[a] Methods are point source (PS), uniform filling (U), and deconvolved (D).

3.1. *LTE Modeling: Optically Thick CO Emission*

Comparing CO(3–2) to the other CO transitions [CO(3–2)/CO(1–0) line ratio is used unless otherwise stated] can, in principle, be used to constrain gas excitation temperatures and optical depths. The ratio of the CO(3–2) intensity to the CO(1–0) intensity under the LTE assumption is

$$\frac{I_{32}}{I_{10}} = \frac{\int T_{32}\, dv}{\int T_{10}\, dv} \simeq \frac{f_{32}[J_{32}(T_{ex}) - J_{32}(T_{cmb})](1 - e^{-\tau_{32}})}{f_{10}[J_{10}(T_{ex}) - J_{10}(T_{cmb})](1 - e^{-\tau_{10}})},$$

where $J_\nu(T_{ex}) = (h\nu/k)/[\exp(h\nu/kT_{ex}) - 1]$, with τ and f being the optical depth and filling factor of each transition,

respectively (e.g., Hurt et al. 1993). To increase the signal-to-noise ratio (SNR), we have used the ratio of integrated intensities instead of the peak main-beam temperatures. This requires that the CO(3–2) and CO(1–0) line profiles be similar. For most of the galaxies this is a good approximation (§ 6). For the LTE approximation, ratios greater than unity indicate warm optically thin gas, while ratios less than unity indicate optically thick molecular gas.

In practice, non-LTE effects, such as different source sizes for the CO(3–2) and CO(1–0) transitions or different T_{ex} for each transition due to temperature gradients and differential optical depth effects in externally heated clouds, may affect the ratio. This data set cannot address such details. A discussion of these details would require higher resolution or observations of rare CO isotopomers. The ^{13}CO isotopomers, whose transitions are less optically thick, can be helpful in better constraining the properties of these galaxies, but unfortunately these galaxies are too weak in ^{13}CO to detect with current telescopes (except He 2-10).

Previous studies indicate that variations in T_{ex} become important in localized regions of high column density, where optical depths of order unity are reached over very small physical distances (e.g., Turner, Hurt, Hudson 1993; Meier, Turner, & Hurt 2000). When averaged over large single-dish beams, the potential error associated with such effects appears to be minor. For example, in the case of the nucleus of the nearby metal-rich starburst IC 342, the physical conditions derived using single-dish ^{12}CO observations (Eckart et al. 1990) are similar to those obtained with higher resolution, even with the presence of strong local temperature gradients (Meier et al. 2000). Similar results have been found from studies of Galactic star-forming regions (e.g., Wilson, Howe, & Balogh 1999).

Nearly all the galaxies we observe have ratios $\lesssim 1.0$, which indicate optically thick emission. NGC 3077 (1.1) and the one velocity component of Haro 3 (1.3) have ratios that are larger than 1, but only marginally so. In the case of NGC 1569 and NGC 3077, some portion of the high line ratios is due to a slightly larger line width of the CO(3–2) line relative to the CO(1–0) lines, indicating that there may be some regions off line center that have CO(3–2)/CO(1–0) ratios greater than 1.0. But in both cases the SNR is too low to say with certainty. It appears that optically thick gas dominates the CO emission in these dwarf galaxies.

We estimate the gas excitation temperatures of the six detected galaxies, assuming the molecular gas is optically thick. Derived T_{ex} values range from ~ 6 K (Haro 2) to greater than 50 K (NGC 1569, NGC 3077, and Haro 3). For the high-ratio galaxies a specific excitation temperature cannot be obtained because the CO(3–2)/CO(1–0) ratio ceases to differentiate temperatures well for $T_k \gtrsim 30$ K. As a result of beam dilution, T_{mb}/T_{ex} yields an estimate of the areal filling factor for each of the galaxies. Rather low filling factors are found, with values ranging from $f_a \sim 0.02$ to less than 0.001 (Table 4).

3.2. *LVG Modeling: Molecular Cloud Densities*

Additional constraints on the physical conditions of the molecular gas can be obtained using a Large Velocity Gradient (LVG) model (Goldreich & Kwan 1974; De Jong, Chu, & Dalgarno 1975). Because of the relatively large Doppler shifts within the cloud, the emergent intensity can be related to its local sources of excitation, T_k and N_{H_2}. As a result, LVG models can be used to get an indication of the gas kinetic temperature and density, given observations of several line ratios or antenna temperatures. While filling factors do not strongly affect the line ratios for our matched beam observations, they do sensitively affect the brightness temperatures. The molecular clouds in these galaxies are unresolved. Therefore, only line ratios provide useful constraints. Detailed LVG modeling is not possible with two line ratios, CO(3–2)/CO(1–0) and CO(2–1)/CO(1–0), since there are three unknowns: the gas density, n_{H_2}, the kinetic temperature, T_k, and $X_{CO}/(dv/dr)$. As mentioned earlier, temperature gradients can also contribute; however, for a reasonable assumption of the abundance per velocity gradient it is possible to provide rough constraints on the physical parameters. Given our limited knowledge of the physical conditions in dwarf starbursts, even rough constraints are important.

The LVG models were run for gas densities ranging from $n_{H_2} = 10^2$ to 10^6 cm^{-3} and kinetic temperatures, T_k, of 1–100 K, for a CO abundance per velocity gradient, $X_{CO}/(dv/dr)$, ranging between 10^{-6} and 10^{-3}. Given that we have only two lines to constrain three variables, model solutions are displayed for only one choice of $X_{CO}/(dv/dr)$. Figure 2 displays the best-fit solutions for T_k and N_{H_2} with an $X_{CO}/(dv/dr)$ estimated in the following manner: the CO

TABLE 4

MOLECULAR GAS PROPERTIES

	He 2-10	NGC 5253	NGC 1569	NGC 3077	Haro 2	Haro 3	II Zw 40	Mrk 86
LTE:								
T_d	43	46	43	34	42	41	48	33
T_{ex}.....	11	15	>50	>50	6	>50	<7	<7
f_a	0.02	0.005	<0.001	<0.002	0.005	<0.001	<0.004	<0.005
$\langle G_o \rangle$[a]	$10^{3.4}$	10^3	$10^{2.5}$	$10^{2.7}$	$10^{3.6}$	$10^{3.3}$	10^3	$10^{2.4}$
LVG:								
T_k	10[b]	30	>40	$\gtrsim$ 20	5	...	...	5
n_{H2}	$\gtrsim 10^{3.5}$[b]	$\sim 10^3$	$>10^{2.5}$	$\gtrsim 10^3$	$\gtrsim 10^4$	...	...	$\gtrsim 10^4$
$\sqrt{n}/T_k$.....	$\gtrsim$5.6[b]	1.0	$\sim$1.5	$\gtrsim$1.5	20	...	...	20
$n_{H2}T_k$.....	$\gtrsim 3 \times 10^4$[b]	3×10^4	$\gtrsim 1 \times 10^5$	$\gtrsim 2 \times 10^4$	$\gtrsim 5 \times 10^4$	...	...	$\gtrsim 5 \times 10^4$

[a] Using the OB association relationship, $\langle G_o \rangle > \simeq 1.2 \times 10^{-6} L_{IR}$ of Wolfire, Tielens, & Hollenbach 1990, with $R = \lambda \sim 100$ pc, which is typical of galactic nuclei. This may be an underestimate of λ and thus of $\langle G_o \rangle$, since these dwarfs are dust-poor and are potentially more "porous" to radiation than metal-rich galaxies; see Petitpas & Wilson 1998.

[b] The χ^2 values of this solution are high, also the ^{13}CO observations are inconsistent with these values (Fig. 2, *top left*; § 6), so this solution should be considered uncertain.

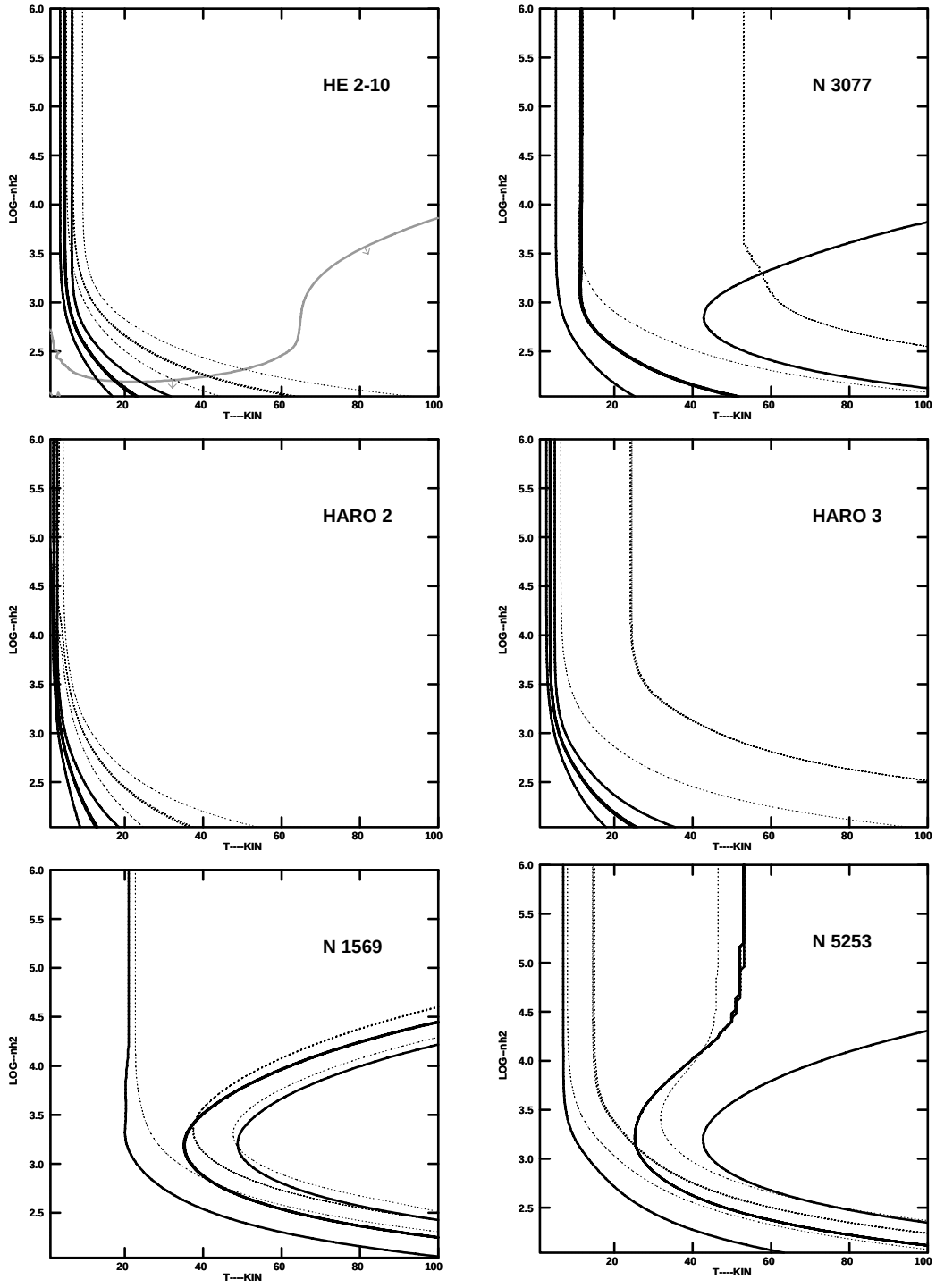

FIG. 2.— LVG models for the six detected galaxies, showing the CO(2–1)/CO(1–0) line ratio (*solid line*) and the CO(3–2)/CO(1–0) line ratio (*dashed line*). For each case, the bold line represents the measured value and the thin lines represent the $\pm 1\sigma$ range. The best-fit solutions are the regions where both line ratios overlap. For all models displayed, the velocity gradient is 1 km s^{-1} pc^{-1}. The [CO/H$_2$] abundances are 8×10^{-5} (1 $Z_\odot$) for He 2-10 and NGC 3077, 2.7×10^{-5} ($\frac{1}{3}$ $Z_\odot$) for Haro 2 and Haro 3, and 1.1×10^{-5} ($\frac{1}{7}$ $Z_\odot$) for NGC 1569 and NGC 5253. For He 2-10, the ^{12}CO(1–0)/^{13}CO(1–0) line ratio was also modeled. The gray curve represents the lower limit of Baas, Israel, & Koornneef 1994 over the same beam size as the CO(3–2) line ratios (consistent with the value obtained by Kobulnicky et al. (1995) over a larger beam size). The abundance per unit velocity gradient used in this model is 5×10^{-7} km s^{-1} pc^{-1}.

abundance is assumed to be the solar CO abundance scaled relative to the galaxies' metallicity and a constant velocity gradient of 1 km s^{-1} pc^{-1}, which should roughly account for metallicity effects (Verter & Hodge 1995; Wilson 1995). The solutions obtained are relatively insensitive to $X_{CO}/(dv/dr)$ as long as it is within a factor 4–5 times the displayed value. For different assumed values of $X_{CO}/(dv/dr)$, the best-fit solutions shift slightly toward higher (lower) densities for lower (higher) values of $X_{CO}/(dv/dr)$ because of the rise in the effective critical density caused by decreased radiative trapping.

Sage et al. (1992) argue that CO(2–1)/CO(1–0) line ratios obtained by approximating the source size as a point source are closer to reality because of the small CO source sizes

expected for dwarf galaxies. The low derived CO(3–2) filling factors appear to confirm this. Therefore, the point-source ratio approximations are used for galaxies with no mapping information (Table 3). The details of the LVG solutions for each galaxy are addressed in § 6, but the basic results can be understood in simple terms. To excite a bright CO(3–2) line the gas must either be warm or have a relatively high density. At high densities the lower J transitions of CO will be thermalized and the CO(2–1)/CO(1–0) and CO(3–2)/CO(1–0) values will just reflect the Rayleigh-Jeans temperature corrections. At low densities, CO(3–2) weakens faster than CO(2–1) because of its higher critical density. Therefore, galaxies with similar CO(2–1)/CO(1–0) and CO(3–2)/CO(1–0) values indicate thermalized, high-density gas (the larger the ratios, the higher the temperature), while in galaxies with CO(3–2)/CO(1–0) < CO(2–1)/CO(1–0) lower density gas is indicated.

The galaxies with low to moderate CO(3–2)/CO(1–0) and CO(2–1)/CO(1–0) values (He 2-10, Haro 2, and Mrk 86) are best fitted by molecular gas that is dense ($n_{H_2} > 10^4$ cm^{-3}) and cold ($T_k > 5$–10 K). The galaxies with high CO(3–2)/CO(1–0) and CO(2–1)/CO(1–0) values (NGC 1569, 3077, and 5253) have a large range of parameter space that fits the observed values. There is a warm, low-density solution ($T_k > 40$ K; $n_{H_2} > 10^{2.5}$ cm^{-3}; NGC 5253) or a warm, high-density solution ($n_{H_2} > 10^{3.5}$ cm^{-3}; NGC 1569, NGC 3077). For the remaining galaxies, Haro 3 and II Zw 40, no constraints can be made (see § 6 for details). Point-source ratios preferentially bias the ratios downward, i.e., toward lower temperatures or lower densities, so these derived values reflect lower limits to the density and temperature if the true source sizes are larger than $\sim 10''$.

Table 4 summarizes the excitation conditions for the eight galaxies. The derived temperatures and densities of the molecular clouds in these dwarf starburst galaxies are different from those found in the Galactic disk and nonstarburst dwarf galaxies but similar to those found in other, higher metallicity, starburst nuclei (e.g., Young & Scoville 1991; Braine & Combes 1992; Wild et al. 1992; Devereux et al. 1994; Aalto et al. 1995; Petitpas & Wilson 1998). Sage et al. (1992) come to a similar conclusion based on CO(2–1).

Despite the low metallicity, strong radiation fields, and weak CO, CO appears not to have become optically thin in the low J transitions of dwarf starbursts. A likely explanation for this is that if the CO column density is high enough to shield itself against photodissociation and hence maintain a detectable amount of CO ($N_{CO} \lesssim 10^{17}$ cm^{-2}; Lequeux et al. 1994), then that column density is high enough for the low J transitions of CO to be optically thick (Pak et al. 1998). Over the region of the starburst where CO can survive, CO might be expected to be optically thick and conditions there to resemble the physical conditions of higher metallicity starbursts, with the difference between the two environments (the weakness of CO in the low-metallicity systems) predominately reflecting increased beam dilution due to smaller CO cloud size (e.g., Maloney & Black 1988; Lequeux et al. 1994; Maloney & Wolfire 1997).

The large optical depths, the relatively high densities derived from LVG modeling, and the small molecular cloud filling factor estimates indicate that the CO cloud size may be smaller in these dwarf starbursts than in spiral starbursts. A similar effect is observed for the LMC and the SMC (Israel et al. 1986; Rubio, Lequeux, & Boulanger 1993; Mochizuki et al. 1994). However, since none of the molecular clouds are resolved here, we cannot say whether this is due to photodissociated CO or is just a reflection of the gas "traced by CO(3–2)" with its larger critical density.

3.3. *Distribution of Warm, Dense Molecular Gas in Dwarf Starbursts*

Since bright CO(3–2) emission requires warmer temperatures and higher densities than CO(1–0), it is expected that CO(3–2)/CO(1–0) would peak in regions of active star formation. There has been some evidence for this in nearby spirals (e.g., Garcia-Burillo, Guelin, & Cernicharo 1993; Wilson, Walker, & Thornley 1997), as well as in some of the nearby, less active dwarfs (Petitpas & Wilson 1998; Mauersberger et al. 1999).

For the two galaxies in the sample with spatial information, He 2-10 and NGC 5253, we investigate the spatial variation in the CO(3–2)/CO(1–0) ratio. In these two galaxies, CO(3–2)/CO(1–0) peaks toward the starburst (Table 5). In the case of the fully mapped galaxy, He 2-10, the CO(3–2) emission is more strongly peaked toward the starburst than is CO(1–0), and the tidal features seen in CO(1–0) (peak C) are less pronounced or missing altogether. Baas et al. (1994) also find indications that the CO(1–0) source size is slightly larger than that of CO(3–2). Likewise for NGC 5253, the CO(2–1)/CO(1–0) value obtained from interferometric data indicates that the ratios along the dust lane peak closest to, although not at, the starburst (Meier & Turner 1998). The CO(3–2) observations demonstrate a similar trend. While the three offset positions are not deep enough to detect CO(3–2), the limits show that CO(3–2) is weaker relative to CO(1–0) farther from the starburst.

To test further the result that CO(3–2) is stronger in the central starburst regions of the sample, we compared the observed line ratios with the physical size covered on the galaxy. The findings are plotted in Figure 3. Note that the beam sizes of He 2-10 and NGC 5253 for the measured line ratios are larger than $22''$ and reflect the CO(1–0) beam size of $40''$ and $44''$, respectively. There is a weak trend (correlation coefficient of $r = -0.83$); the line ratio decreases as the physical area on the starburst galaxy

TABLE 5

OFF-CENTER LINE RATIOS

Galaxy and Location	CO(3–2)/CO(1–0)
He 2-10:	
(20, −10)	0.35 ± 0.1
D (20, 10)	0.30 ± 0.1
C (10, −10)	0.35 ± 0.1
NGC 5253:	
(10, −10)	<0.7
(20, 20)	<0.6
(15, 25)	<1.2

NOTE.—Ratios are based on the CO(1–0) interferometer maps at $22''$ resolution and have been corrected for resolved outflux (He 2-10, 82%, Kobulnicky et al. 1995; NGC 5253, 50%, Turner et al. 1997). Uncertainties for the CO(3–2) data are given in Table 3, while the interferometric data are assumed to have an uncertainty of 20%. In the case of NGC 5253 the ratio is that of peak T_{mb} since these three CO(3–2) pointings are nondetections: quoted values are 3 σ upper limits.

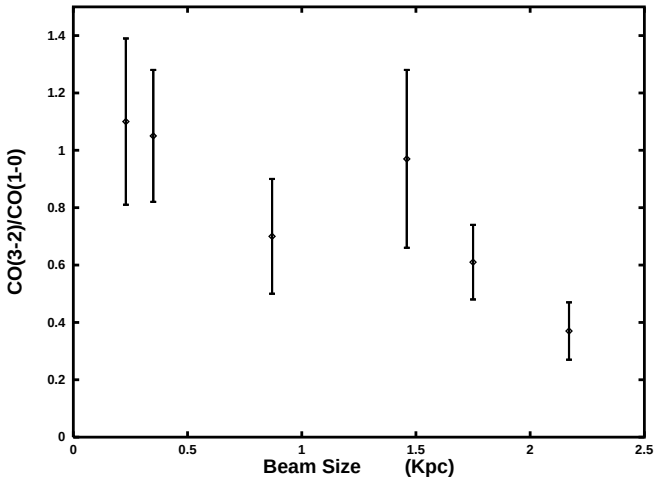

FIG. 3.—CO(3–2)/CO(1–0) line ratio as a function of the projected physical size of the beam over which the ratio has been measured, for the galaxies detected from our sample. A weak correlation is seen.

increases, which implies that including gas in the beam from farther out in the galaxy lowers the ratio. (Haro 3 appears to be somewhat of an exception, but the line ratio of this galaxy appears contaminated by an optically thin velocity component; § 6.) This is consistent with the notion that the highest temperatures and densities are concentrated toward the starburst, with lower temperatures and gas densities over the rest of the galaxy. We conclude that this is a general feature among dwarf starbursts and that the properties derived using the higher J transitions of CO probably better represent the region directly associated with the star formation.

4. MASSES, COLUMN DENSITIES, AND CONVERSION FACTORS

Estimating molecular gas masses in dwarf galaxies can be a particularly tricky business. Dwarf galaxies seem to have a higher standard conversion factor ($X_{\rm CO}$, where $X_{\rm CO} = N({\rm H_2})/I_{\rm CO}$) than do large metal-rich spirals (Israel 1986; Maloney & Black 1988; Elmegreen 1989; Verter & Hodge 1995; Wilson 1995; Arimoto, Sofue, & Tsujimoto 1996). Several methods are used to obtain molecular mass estimates. One is to assume that the molecular clouds are in virial equilibrium and that the line width is representative of the cloud mass. However, because of the large beam sizes of single-dish observations, galaxy rotation contributes significantly to the line width. In fact, it is more likely that the mass measured in this fashion represents an estimate of the *dynamical* mass over the beam. A second method for estimating molecular mass is to assume CO is optically thin and "count molecules" (including He; e.g., Rohlfs & Wilson 1996, p 191) using

$$M_{\rm thin} = 173\ M_\odot \frac{8.5\times10^{-5}}{[{\rm CO/H_2}]} \frac{e^{33.2/T_{\rm ex}}}{e^{16.6/T_{\rm ex}}-1} \times D^2_{\rm mpc} \frac{\int T_{\rm mb}\,dv}{1\ {\rm K\ km\ s^{-1}}},$$

where the value is scaled relative to the Galactic $[{\rm CO/H_2}]$ abundance ratio 8.5×10^{-5} (Frerking, Langer, & Wilson 1982). This method underestimates the total molecular mass, both because the CO emission is optically thick (§ 3.1) and because the CO abundances, $[{\rm CO/H_2}]$, are probably lower than the Galactic value for most of the dwarf galaxies. In addition, molecular masses can be estimated using a metallicity-scaled conversion factor. We use

$$M_{\rm mol} = 1.23\times10^4 \left(\frac{X_{\rm CO}}{X_{\rm COgal}}\right)\left(\frac{115\ {\rm GHz}}{\nu}\right)^2 D^2_{\rm mpc}\,\frac{S_{\rm CO}}{R}\ M_\odot,$$

where $X_{\rm COgal} = 2.3\times10^{20}\ {\rm cm^{-2}}\ ({\rm K\ km\ s^{-1}})^{-1}$ (Strong et al. 1988), $S_{\rm CO}$ is the CO(3–2) flux in Jy km s^{-1} (where a conversion factor of 47.3 Jy K^{-1} is assumed), and R is the CO(3–2)/CO(1–0) line ratio (Wilson et al. 1988; Petitpas & Wilson 1998). The scaling for the conversion factor is quite uncertain because of the few data points, but we estimate it based on the relationship derived from single-dish data (Arimoto et al. 1996).

Collected in Table 6 are the masses derived for each galaxy by the three different methods. We also compare the derived masses with the dust mass estimated from the 100 μm IRAS fluxes (Thronson & Telesco 1986; Melisse & Israel 1994). The virial theorem yields a much larger mass than any of the other methods, consistent with it tracing dynamical mass. It should give a firm upper limit to the molecular mass present. The mass estimates obtained by assuming the CO(3–2) emission is optically thin are more than 100 times lower than those estimated from the conversion factor method. The $M_{\rm thin}$ estimate yields a firm lower limit to the amount of molecular gas. The conversion factor

TABLE 6

GAS MASSES

Galaxy	$T_{\rm ex}$ (K)	$\frac{X}{X_{\rm Gal}}$ [a]	$\frac{M_{\rm vir}}{\sin^2 i}$ [b] ($10^6\ M_\odot$)	$\frac{M_{\rm thin}}{[{\rm CO/H_2}]}$ ($10^6\ M_\odot$)	$M_{\rm mol}$ ($10^6\ M_\odot$)	$\frac{M_{\rm mol}}{M_{\rm vir}}\sin^2 i$	$\frac{M_{\rm mol}}{M_D}$	$\frac{M_{\rm gas}}{M_{\rm vir}}\sin^2 i$ [c]
He 2-10	11	1.0	330	1.0	140	0.42	475	1.4
NGC 5253	15	7.0	94	0.004	37	0.39	680	2.5
NGC 1569	50	5.7	26	0.007	4.6	0.18	140	3.1
NGC 3077	50	0.9	93	0.04	4.4	0.05	45	8.6
Haro 2	6	3.5	1100	2.1	750	0.68	2300	1.1
Haro 3	50	3.5	430	0.25	110	0.26	790	1.7
II Zw 40	...	6.1	...	...	<0.4	...	<830	...
Mrk 86	...	7.7	...	...	<0.3	...	<340	...

[a] Using the single-dish X vs. metallicity relation of Arimoto et al. 1996, $\log(X/X_{\rm Gal}) = -[{\rm O\backslash H}] + 8.93$.
[b] Using $M_{\rm vir} = 210 R_{\rm pc} \Delta V^2_{1/2}\ M_\odot$ from MacLaren, Richardson, & Wolfendale 1988.
[c] $M_{\rm gas} = M_{\rm mol} + M_{\rm H\,I}$; see Table 1.

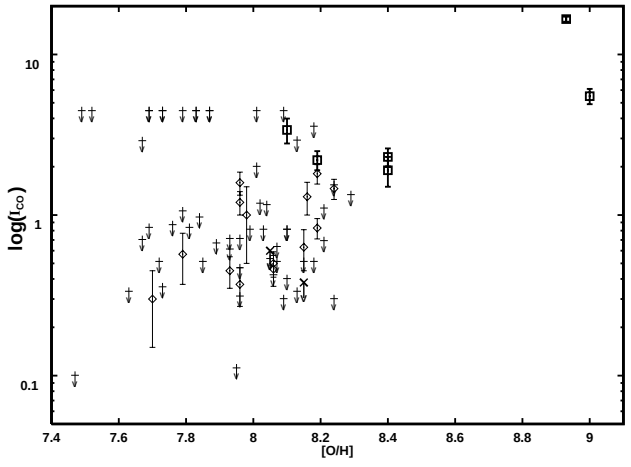

FIG. 4.—CO(3–2) intensity in K km s^{-1} plotted vs. metallicity, showing CO(3–2) detections (*squares*) and upper limits (*crosses*). For reference, the data are plotted over the dwarf galaxy CO(1–0) spectra compiled from the literature by Taylor, Kobulnicky, & Skillman (1998), in which diamonds represent detections and the arrows are upper limits.

method is intermediate between the other two. Therefore, even with its large uncertainty, the best estimate is probably still the conversion factor–based estimate. Since none of the molecular clouds are resolved spatially or in velocity, a detailed investigation of the X_{CO} must await higher resolution. The CO(3–2) data do, however, appear consistent with the I_{CO} versus metallicity relationship found from CO(1–0) for dwarf and spiral galaxies (Fig. 4; Verter & Hodge 1995; Wilson 1995; Arimoto et al. 1996).

5. CO AND DUST: PREFERENTIAL CO DEPLETION?

A correlation between CO and IR luminosity for large starbursts has been known for some time (see the Young & Scoville 1991 review and the references therein). In Figure 5, the infrared luminosity of this sample plus the Mauersberger et al. (1999) sample of nondwarf nuclei are plotted versus their CO(3–2) luminosity. The CO(3–2) data for the dwarf starbursts also show a tight correlation between

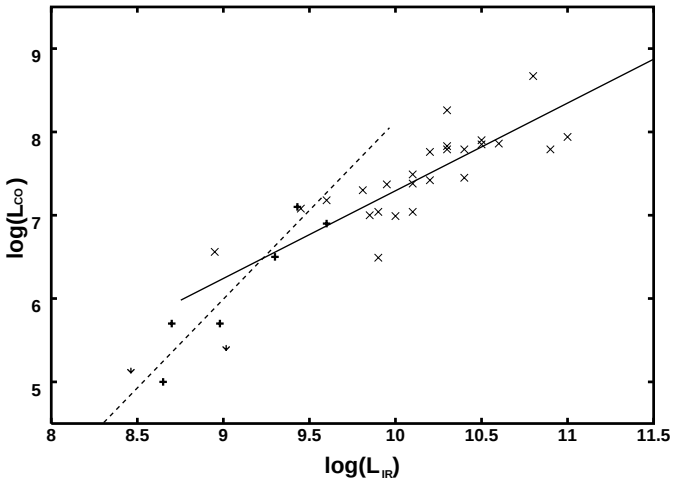

FIG. 5.—Luminosity of CO(3–2) in units of K km s^{-1} pc^{-2} plotted vs. the infrared luminosity in units of $L_\odot$, for the dwarf galaxies (*plus signs*) and for a sample of nondwarf galactic nuclei (*crosses*; Mauersberger et al. 1998). The dashed line is the least-squares fit to the dwarf galaxy sample, and the solid line is the least-squares fit to the spiral nuclei sample.

L_{CO32} and L_{IR}, with the relation

$$\log (L_{IR}) = (6.31 \pm 0.5) + (0.46 \pm 0.08) \log L_{CO32}$$

(correlation coefficient $r = -0.94$). This can be compared with the correlation we calculate using the Mauersberger et al. (1999) data set:

$$\log L_{IR} = 3.20 + 0.93 \log L_{CO32} .$$

In dwarf starbursts, CO emission appears weaker relative to the infrared emission than that in the high-metallicity galaxies. The slope of this relationship is substantially steeper than that found from nearby high-metallicity starburst spirals. The most metal-rich galaxies in this sample follow the relationship found for nondwarfs, but the lower metallicity sources are weaker in L_{CO32} relative to dust than those that would be extrapolated from nondwarfs. While the sample of dwarf galaxies is too small to prove this fact conclusively, it indicates that there may be a break in the slope of L_{CO32} versus L_{IR} at the faint, low-metallicity end. Taylor, Kobulnicky, & Skillman (1998) also suggest a rapid falloff in L_{CO} at metallicities of about 1/10 $Z_\odot$, based on a different line of reasoning. Further observations are key to investigating the validity of this trend.

The weakening of L_{CO} relative to L_{IR} is not necessarily unexpected because of the strong radiation field and low metallicity of these dwarf starbursts. These simultaneously lead to higher dust temperatures and hence L_{IR} and to increased CO photodissociation. Dust survives longer than CO in strong radiation fields, so CO should disappear faster than dust.

6. NOTES ON THE INDIVIDUAL GALAXIES

He 2-10: In Figure 6, the channel maps of He 2-10 are presented. A 14 point map of He 2-10 was made on a 10″ grid in right ascension and declination around the brighter optical starburst component (Vacca & Conti 1992). The $(\Delta\alpha, \Delta\delta) = (0, 0)$ position of He 2-10 was reobserved on February 25 to confirm its line strength. Pointings were extended toward the southeastern portion of the galaxy where a barlike tidal feature is seen in the CO(1–0) interferometer map (Kobulnicky et al. 1995). We detect emission in every position except (20″, 0). The peak T_{mb} occurs at the central position and has the value 0.27 K. This value is about 80% of the value Baas et al. (1994) find for CO(3–2) after we convolve to the same beam size. The CO(3–2) emission at this position has a $V_{FWHM} \sim 57$ km s^{-1} centered at 849 km s^{-1}, with detectable emission spanning a velocity range of 810–890 km s^{-1} (LSR).

We do not detect any obvious emission to a level of 40 mK associated with the kinematically distinct feature labeled "C" by Kobulnicky et al. (1995). There is some hint of a southeastern extension seen at 853 and 861 km s^{-1}, but this is separated by better than two channels (16 km s^{-1}) from their velocity and is not likely to be the same source. On the other hand, we do detect emission that matches both in position and velocity space with the weak detached feature seen in the Kobulnicky et al. (1995) interferometric CO(1–0) map. Kobulnicky et al. (1995) questionably interpret this detached feature as noise, but since we see indications of emission in CO(3–2) at the same location and velocities, this feature may be real. This feature is weak, with $T_{mb} \sim 0.08$ K, and centered at $(\alpha, \delta) = (8^h34^m08^s.65, -26°13'56''.5)$.

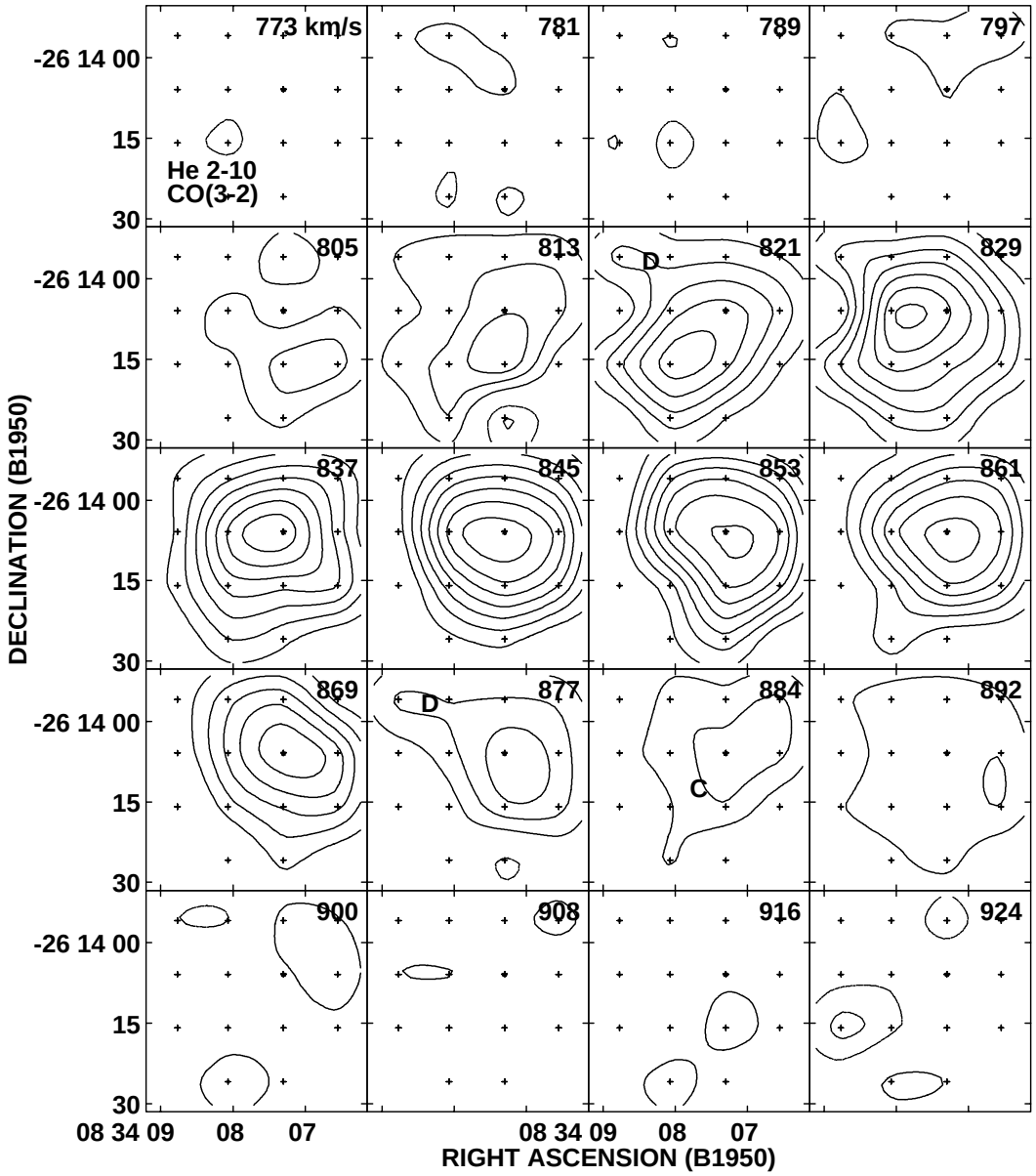

FIG. 6.—Channel maps of He 2-10, showing the V_{LSR} of each channel in each frame (*top right*), the location of the optical starburst and center position (0, 0) (*asterisk*), and additional pointings (*crosses*). Panels are displayed in intervals of 7.8 km s^{-1}. Contours are 1, 2, . . . , and 8 times the 2 σ temperature, 0.035 K. The feature denoted by Kobulnicky et al. (1995) as "C" is labeled "C" at its correct location and velocity, and the location and the two velocities contributing to the "detached" feature are labeled "D" (Kobulnicky et al. 1995).

Figure 7 shows the integrated CO(3–2) intensity map of the nuclear region of He 2-10. The emission from the central peak is more dominant than in CO(1–0). Within pointing uncertainties, the peak of the integrated intensity coincides with the position of the brighter optical starburst component. Of the three extensions seen, one extends to the northeast along P.A $\simeq 50°$, while the other two extend to the southeast. We interpret the two extensions to the southeast as one feature along P.A. $= 130°$ and attribute the apparent split into two features to the lack of a pointing at $(20'', -20'')$. This extension matches what is observed in the interferometric CO(1–0) and CO(2–1) maps and is near the site of an offset star cluster (Kobulnicky et al. 1995; Beck & Kovo 1999; Meier & Turner 1998).

The centrally peaked component has an FWHM of $26''$. When deconvolved from the beam, we estimate that the source size is $13'' \pm 3''$ (560 ± 110 pc at 9 Mpc). Since the observations of Baas et al. (1994) are at a different resolution than ours, we can compare the observed main-beam temperatures to get a second estimate of the source size. Again, $13''$ is obtained. Because both methods agree and are consistent with the size estimated from the high-resolution interferometer CO(2–1) map (Meier & Turner 1998), we conclude that this is a good representation of the CO(3–2) source size.

Assuming a source size of $13''$ for He 2-10, we obtain CO(3–2)/CO(2–1), CO(3–2)/CO(1–0), and CO(2–1)/CO(1–0) line ratios of 1.0 ± 0.2, 0.61 ± 0.1, and 0.59 ± 0.1, respectively. These are slightly lower than the previous results of Baas et al. (1994). The value CO(3–2)/CO(2–1) > 1.0 combined with a high $^{12}CO/^{13}CO$ isotopic ratio led them to conclude that the CO emission is optically thin. With the

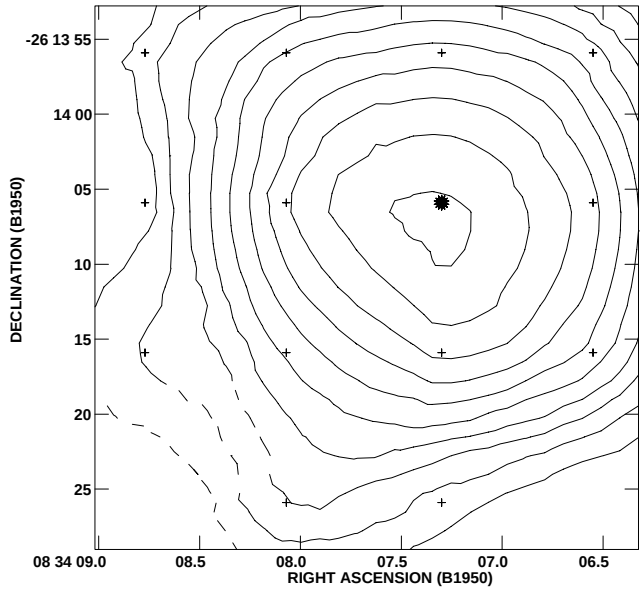

FIG. 7.—Integrated intensity map of He 2-10, showing the location of the optical starburst and center pointing (0, 0) (*asterisk*) and additional pointings (*crosses*). The integrated intensity map was mapped from only the channels displayed in Fig. 2 (773 to 924 km s^{-1}). Emission below 1.3 σ in each channel map was cut. Contours are 1, 2, . . . , and 10 times the 2 σ value, 1.6 K km s^{-1}. The map is uncertain at (20″, −20″) because there is no observation there. To represent this fact the contours are dashed.

advantage of a fully sampled map and CO(3–2) observations with beam matched to their $J = 2$–1 observations, these observations do not necessarily require optically thin gas. LVG modeling yields a best-fit solution of $n_{H_2} > 10^{3.5}$ cm^{-3} and $T_k \sim 5$–10 K, however, the χ^2 for the solution is high. These gas temperatures are slightly cooler than the $\sim$20 K estimated from LTE modeling. The ^{12}CO(1–0)/^{13}CO(1–0) line ratio was also modeled. A model with [^{12}CO/^{13}CO] = 40 and $dv/dr = 1$ km s^{-1} pc^{-1} and a ^{13}CO depleted model with [^{12}CO/^{13}CO] = 120 were run (Fig. 2). Both CO abundance models are inconsistent with the solution found from the ^{12}CO transitions. The ^{13}CO line in He 2-10 is too weak (^{12}CO(1–0)/^{13}CO(1–0) $\lesssim$ 22) relative to that predicted from the ^{12}CO lines, as Baas et al. (1994) noted. To have ^{12}CO(1–0)/^{13}CO(1–0) $\sim$ 22, the ^{12}CO lines must be optically thin, unless the abundance is *severely* depleted. However, nowhere over the CO(3–2) solution space is the modeled ^{12}CO optically thin. Therefore, given that the χ^2 for the ^{12}CO solution is high and that the ^{13}CO observations are not consistent with the simple LVG modeling, the solution should be considered uncertain. ^{13}CO is probably preferentially photodissociated or source sizes are much smaller in ^{13}CO than ^{12}CO. As far as the high isotopic ratios obtained are concerned (Baas et al. 1994; Kobulnicky et al. 1995), the optically thinner ^{13}CO lines are less capable of self-shielding than ^{12}CO and are likely to be preferentially photodissociated by the intense radiation fields. So the abundance and spatial extent of ^{13}CO may be greatly diminished with respect to ^{12}CO (e.g., van Dishoeck & Black 1988; Lequeux et al. 1994; Warin, Benayoun, & Viala 1996).

NGC 5253: The four pointings for NGC 5253 were chosen based on the CO(1–0) interferometric map made at Owens Valley Millimeter Observatory (OVRO) (Turner, Beck, & Hurt 1997). We observed two pointings associated with the central dust lane and two toward a possible molecular cloud at the edge of the OVRO primary beam. In Figure 8, the four CO(3–2) and one CO(2–1) spectra are overlaid on the OVRO CO(1–0) map (Fig. 2 of Turner et al. 1997). The measured CO(3–2) intensity is about 5–6 σ, and both the velocity centroid ($V_o \sim 420$ km s^{-1}) and the line width ($\Delta V_{FWHM} \sim 45$ km s^{-1}) match published single-dish CO(1–0) detections (Wiklind & Henkel 1989; Taylor et al. 1998). For the three other spectra there are no detections to 3 σ. LVG modeling yields densities of $n_{H_2} > 10^{2.5}$ cm^{-3} and $T_k > 40$ K, with the best-fit solutions obtained for the lower densities.

NGC 1569: We detect CO(3–2) in this galaxy with $I_{CO} =$ 2.2 K km s^{-1} ($T_{mb} = 63$ mK) toward H II region C (Waller 1991). This corresponds to the central position observed by Greve et al. (1996) in CO(1–0) and CO(2–1). The line width of CO(3–2) is slightly larger (32.3 km s^{-1}) than that of the CO(1–0) observations (23.6 km s^{-1}). The line center is shifted to slightly higher velocities than the CO(1–0) [−69 relative to −81 km s^{-1} for CO(1–0)]. The CO(2–1) line center is intermediate between the two, 78.4 km s^{-1}. Therefore, while the velocity centroids are roughly consistent, there is a marginal trend that the emission from the higher J transitions tends toward increasing velocity. Comparing these higher velocities with the velocity field obtained from H I (Reakes 1980; Stil & Israel 1998) indicates that CO(3–2) peaks slightly closer to the super–star cluster, A, than does CO(1–0) and is probably associated with GMC 2 of Taylor et al. (1999).

Interestingly, there is a secondary peak seen at −140 km s^{-1}. This peak is at the 4 σ level, and the line profile is similar to the main peak. H I is also present at this velocity, giving more evidence that this feature may be real. We have inspected the CO(1–0) and CO(2–1) spectra of Young et al. (1984), Taylor et al. (1998), and Greve et al. (1996) for similar features. Unfortunately, the spectra of Greve et al. (1996) do not extend that far in velocity, and while the Young et al. (1984) spectrum shows indications of a feature at this velocity, it does not seem to be confirmed by the more sensitive observations of Taylor et al. (1998). Therefore, until further observations can be obtained, we assume it is not real. Since both the CO(3–2)/CO(1–0) and the CO(2–1)/CO(1–0) line ratios are $\simeq$1, a large region of parameter space is acceptable to the LVG models. The best fits are represented an arch running from $T_k \sim 100$ K and $n_{H_2} \simeq 10^{4.5}$ cm^{-3} down to $T_k \sim 40$ K and $n_{H_2} \simeq 10^{3.5}$ cm^{-3} and back over to $T_k \sim 100$ K and $n_{H_2} \simeq 10^{2.4}$ cm^{-3}.

NGC 3077: Observations were centered on the location of the interferometer CO(2–1) peak (Meier & Turner 2001). This is equivalent to the (−10, 0) position of Becker et al. (1989). The CO(3–2) line width of 51 km $^{-1}$ is slightly wider than that observed by Becker et al. (1989) in CO(1–0) (34 km s^{-1}), while the centroid is consistent with that observed in the lower transitions. Based on the CO(2–1)/CO(1–0) line ratio discussed in Becker et al. (1989), we estimate a CO(3–2)/CO(1–0) line ratio of 1.1. Becker et al. (1989) obtain a CO(2–1)/CO(1–0) line ratio of 0.82. For NGC 3077, the best-fit LVG solution corresponds to $T_k \sim 30$ K and $n_{H_2} > 10^{3.5}$ cm^{-3}, with an acceptable range of solutions covering $T_k > 20$ K and $n_{H_2} > 10^3$ cm^{-3}.

Haro 2: We observed CO(3–2) at the same position as CO(1–0) and CO(2–1) of Sage et al. (1992). The fitted line width is 69 km s^{-1}, but the line appears distinctly non-Gaussian. The SNR of the spectrum is too low to warrant

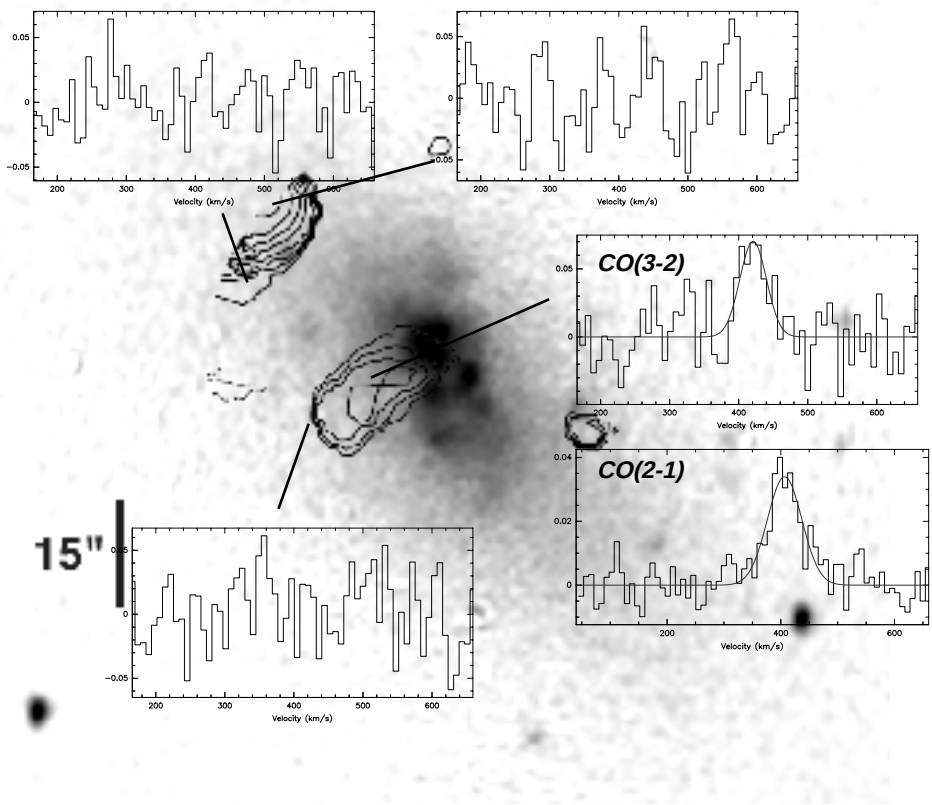

FIG. 8.—Spectra of NGC 5253 overlaid on the OVRO millimeter interferometer CO(1–0)/red image of Turner, Beck, & Hurt (1997, their Fig. 2). Each observation is displayed with a line running from the spectrum to the location at which it was obtained. The main-beam temperature (*vertical axis*) ranges from −0.065 to 0.065 K. Velocity ranges from 180 to 620 km s^{-1} (*horizontal axis*). The spectra are Hanning smoothed to a velocity resolution of 8 km s^{-1}. For the central position the new CO(2–1) spectrum is included under the CO(3–2) spectra. For the detections the best–fit Gaussian is displayed.

any multicomponent fit, but the spectrum is consistent with two roughly equal intensity Gaussians separated by about 40 km s^{-1}. For Haro 2, the best-fit solution obtained from LVG modeling is $n_{H_2} > 10^4$ cm^{-3} and $T_k \sim 5$ K, but the χ^2 values are high, similar to that found for He 2-10. However, the low ratios obtained for both transitions require that T_k be low and n_{H_2} be high.

Haro 3 (*NGC 3353*): CO(3–2) observations are centered on starburst region B (Steel et al. 1996). The fitted Gaussian yields a line width of 53 km s^{-1}, which is slightly narrower than that for CO(1–0) ($\Delta v_{10} = 64$ km s^{-1}; Sage et al. 1992). The CO(3–2) spectrum shows a narrow brighter component at 960 km s^{-1} ($v_{LSR} = 950$ km s^{-1}). The same peak is seen in both the CO(1–0) and CO(2–1) spectra of Sage et al. (1992) and matches the velocity of Hα at the starburst region, B1, of Steel et al. (1996). Therefore, we conclude this feature is real. By inspecting the spectra of Sage et al. (1992) a main-beam temperature ratio of 1.3 is estimated for this component. The large CO(3–2)/CO(1–0) line ratio is inconsistent with any region of parameter space indicated by the CO(2–1)/CO(1–0) line ratio, so no LVG solution is found. This component is potentially optically thin and may be causing an overestimate of the global CO(3–2)/CO(1–0) ratio in Haro 3.

II Zw 40: The beam was centered on the star formation peak and is within an arcsecond of the observed CO(2–1) and CO(1–0) position of Sage et al. (1992). The line is not detected. Our limit for the CO(3–2) main-beam temperature is 7 mK. There appears to be no hint of a line at the 1 σ level in either of the previously published CO(1–0) velocity centroids, $\sim$770 km s^{-1} (Sage et al. 1992) or $\sim$850 km s^{-1} (Tacconi & Young 1987). LVG modeling does not provide a useful constraint on the gas properties because CO(3–2) is not detected. The low CO(3–2)/CO(1–0) ratio implies that the molecular gas must not be very warm and dense.

Mrk 86 (*NGC 2537*): We do not detect any CO(3–2) emission to a limit of 11 mK. Sage et al. (1992) detected weak CO(1–0) and CO(2–1) at a V_{LSR} of 460 km s^{-1}. There is a hint of a very weak line at $V_{LSR} = 428$ km s^{-1}, but it is only at 1.5 σ. The low CO(3–2)/CO(1–0) ratio limit and the low CO(2–1)/CO(1–0) ratio imply LVG fits quite similar to those of Haro 2.

7. CONCLUSIONS

We have observed CO(3–2) in a sample of eight dwarf galaxies with very intense recent star formation. The galaxies range in metallicity from 1 to $\sim$0.1 $Z_\odot$. CO(3–2) was detected in six of the eight galaxies. The galaxies are all quite weak ($T_{mb} \sim 50$ mK), with the exception of He 2-10, which was mapped. The two galaxies not detected (II Zw 40 and Mrk 86) are two of the lowest-metallicity galaxies.

The CO(3–2)/CO(1–0) line ratio ranges from 0.37 to 1.1 for the six detected galaxies. With the possible exception of one velocity component in Haro 3, all the galaxies appear dominated by optically thick CO emission, even though they have low metallicity and strong radiation fields. This is consistent with the fact that CO can survive intense radiation fields only where it is self-shielded and thus optically thick.

The error-weighted mean CO(3–2)/CO(1–0) line ratio is 0.60 ± 0.06. This is virtually identical to that seen in high-metallicity starbursts. While CO(3–2) is very weak on an absolute scale, it is as bright relative to CO(1–0) as in high-metallicity starbursts. In general, in terms of the physical properties of the molecular gas, dwarf starbursts do not appear to be particularly unusual examples of the starburst family. They appear to be similar to their high-metallicity counterparts, with the exception that CO has a smaller filling factor and hence weaker intensities.

LVG models from the CO line ratios imply that for He 2-10, Haro 2, and Mrk 86, the molecular gas traced by CO is cool ($T_k \sim 10$ K) and dense ($n_{H_2} \lesssim 10^4$ cm^{-3}). For NGC 5253, the molecular gas appears warm ($T_k > 40$ K) and moderately dense ($n_{H_2} \lesssim 10^{2.5}$–$10^3$ cm^{-3}). The molecular gas in NGC 1569 and NGC 3077 is also warm but somewhat more dense ($n_{H_2} > 10^4$ cm^{-3}).

For the two galaxies that have been observed with multiple pointings, He 2-10 and NGC 5253, we find that the CO(3–2)/CO(1–0) line ratio decreases away from the starburst. The entire sample shows a trend in which the ratio is lower for the galaxies when the beam includes more "nonstarburst" gas (i.e., covers larger fractions of the galaxy). This is interpreted as due to a drop in gas temperature and density away from the starburst.

The combination of low filling factors derived from the CO(3–2) emission, the fact that CO(3–2) systematically remains optically thick in spite of low metallicities and strong radiation fields, and a trend found between L_{CO} and L_{IR} implies that the lower metallicity galaxies are more strongly depleted in CO relative to dust than higher metallicity galaxies are.

We gratefully thank Tom Phillips, Dominic Benford, and Atilla Kovacs for useful discussions and help in making the observations. We thank Gene Serabyn for obtaining the CO(2–1) spectrum of NGC 5253. We also thank Chip Kobulnicky for useful discussions and providing us with the OVRO CO(1–0) data for He 2-10. We also thank the referee, Christine Wilson, for many helpful comments. This work was supported in part by NSF grant AST 94-17968 and by the Sackler Center for Astronomy at Tel Aviv University. This research has made use of the NASA/IPAC extragalactic database.

REFERENCES

Aalto, S., Booth, R. S., Black, J. H., & Johansson, L. E. B. 1995, A&A, 300, 369
Arimoto, N., Sofue, Y., & Tsujimoto, T. 1996, PASJ, 48, 275
Arnault, P., Casoli, F., Combes, F., & Kunth, D. 1988, A&A, 205, 41
Arp, H., & Sandage, A. 1985, AJ, 90, 1163
Baas, F., Israel, F. P., & Koornneef, J. 1994, A&A, 284, 403
Beck, S. C., & Kovo, O. 1999, AJ, 117, 190
Becker, R., Schilke, P., & Henkel, C. 1989, A&A, 211, L19
Braine, J., & Combes, F. 1992, A&A, 264, 433
Conti, P. S. 1991, ApJ, 377, 115
Conti, P. S., & Vacca, W. D. 1994, ApJ, 423, L97
Cottrell, G. A. 1976, MNRAS, 174, 455
De Jong, T., Chu, S.-I., & Dalgarno, A. 1975, ApJ, 199, 69
Devereux, N., Yoshiaki, T., Sanders, D. B., Nakai, N., & Young, J. S. 1994, AJ, 107, 2006
Eckart, A., Downes, D., Genzel, R., Harris, A. I., Jaffe, D. T., & Wild, W. 1990, ApJ, 348, 434
Elmegreen, B. G. 1989, ApJ, 338, 178
Frerking, M. A., Langer, W. D., & Wilson, R. W. 1982, ApJ, 262, 590
Gallagher, J. S., & Hunter, D. A. 1984, ARA&A, 22, 37
Garcia-Burillo, S., Guelin, M., & Cernicharo, J. 1993, A&A, 274, 123
Garnett, D. R. 1990, ApJ, 363, 142
Goldreich, P., & Kwan, J. 1974, ApJ, 189, 441
Gonzalez Delgado, R. M., Leitherer, C., Heckman, T., & Cervino, M. 1997, ApJ, 483, 705
Greve, A., Becker, R., Johansson, L. E. B., & McKeith, C. D. 1996, A&A, 312, 391
Heckman, T. M. 1980, A&A, 87, 142
Hodge, P. W. 1971, ARA&A, 9, 35
Hurt, R. L., Turner, J. L., Ho, P. T. P., & Martin, R. N. 1993, ApJ, 404, 602
Israel, F. P. 1986, A&A, 168, 369
———. 1988, A&A, 194, 24
Israel, F. P., & de Bruyn, A. G. 1988, A&A, 198, 109
Israel, F. P., De Gwaauw, T., Van de Stadt, H., & De Vries, C. P. 1986, ApJ, 303, 186
Israel, F. P., & van Driel, W. 1990, A&A, 236, 323
Klein, U., Weiland, H., & Brinks, E. 1991, A&A, 246, 323
Kobulnicky, H. A., Dickey, J. M., Sargent, A. I., Hogg, D. E., & Conti, P. S. 1995, AJ, 110, 116
Kobulnicky, H. A., & Johnson, K. 1999, ApJ, 527, 154
Kobulnicky, H. A., Kennicutt, R. C., & Pizagno, J. L. 1999, ApJ, 514, 544
Kobulnicky, H. A., & Skillman, E. D. 1995, ApJ, 454, L121
———. 1997, ApJ, 489, 636
Kunth, D., & Jobert, M. 1985, A&A, 142, 411
Lequeux, J., Le Bourlot, J., Pineau Des Forets, G., Roueff, E., Boulanger, F., & Rubio, M. 1994, A&A, 292, 371
MacLaren, I., Richardson, K. M., & Wolfendale, A. W. 1988, ApJ, 333, 821
Maloney, P., & Black, J. H. 1988, ApJ, 325, 389
Maloney, P., & Wolfire, M. G. 1997, in IAU Symp. 170, CO: Twenty-Five Years of Millimetre-Wave Spectroscopy, ed. W. B. Latter, S. J. E. Radford, P. R. Jewell, J. G. Mangum, & J. Bally (Dordrecht: Kluwer), 299
Marconi, G., Matteucci, F., & Tosi, M. 1994, MNRAS, 270, 35
Mauersberger, R., Henkel, C., Walsh, W., & Schulz, A. 1999, A&A, 341, 256
Meier, D. S., & Turner, J. L. 1998, in IAU Symp. 193, Wolf-Rayet Phenomena in Massive Stars and Starburst Galaxies, ed. K. A. van der Hucht, G. Koenigsberger, & P. R. J. Eenens (San Francisco: ASP), 746
———. 2001, in preparation
Meier, D. S., Turner, J. L., & Hurt, R. L. 2000, ApJ, 531, 200
Melisse, J. P. M., & Israel, F. P. 1994, A&AS, 103, 391
Meurer, G. R., Heckman, T. M., Leitherer, C., Kinney, A., Robert, C., & Garnett, D. R. 1995, AJ, 110, 2665
Mochizuki, K., et al. 1994, ApJ, 430, L37
Niklas, S., Klein, U., Braine, J., & Wielebinski, R. 1995, A&AS, 114, 21
Pak, S., Jaffee, D. T., van Dishoeck, E. F., Johansson, L. E. B., & Booth, R. S. 1998, ApJ, 498, 735
Petitpas, G. R., & Wilson, C. D. 1998, ApJ, 496, 226
Reakes, M. 1980, MNRAS, 192, 297
Rohlfs, K., & Wilson, T. L. 1996, Tools of Radio Astronomy (2d ed.; Berlin: Springer)
Rubio, M., Lequeux, J., & Boulanger, F. 1993, A&A, 271, 9
Sage, L. J., Salzer, J. J., Loose, H.-H., & Henkel, C. 1992, A&A, 265, 19
Sandage, A. 1994, ApJ, 423, L13
Sanders, D. B., Tilanus, R. P. J., Scoville, N. Z., Wang, Z., & Zhou, S. 1993, in Back to the Galaxy, ed. F. Verter (Dordrecht: Kluwer), 21
Schaerer, D., Contini, T., & Pindao, M. 1999, A&AS, 136, 35
Skillman, E. D., Kennicutt, R. C., & Hodge, P. W. 1989, ApJ, 347, 875
Steel, S. J., Smith, N., Metcalfe, L., Rabbette, M., & McBreen, B. 1996, A&A, 311, 721
Stil, J. M., & Israel, F. P. 1998, A&A, 337, 64
Strong, A. W., et al. 1988, A&A, 207, 1
Tacconi, L. J., & Young, J. S. 1987, ApJ, 322, 681
Tammann, G., A., & Sandage, A. 1968, ApJ, 151, 825
Taylor, C. L., Hüttemeister, S., Klein, U., & Greve, A. 1999, A&A, 349, 424
Taylor, C. L., Kobulnicky, H. A., & Skillman, E. D. 1998, AJ, 116, 2746
Thronson, H. A., & Telesco, C. M. 1986, ApJ, 311, 98
Thuan, T. X., & Martin, G. E. 1981, ApJ, 247, 823
Turner, J. L., Beck, S. C., & Hurt, R. L. 1997, ApJ, 474, L11
Turner, J. L., Ho, P. T. P., & Beck, S. C. 1998, AJ, 116, 1212
Turner, J. L., Hurt R. L., & Hudson, D. Y. 1993, ApJ, 413, L19
Vacca, W. D., & Conti, P. S. 1992, ApJ, 401, 543
van Dishoeck, E. F., & Black, J. H. 1988, ApJ, 334, 771
Verter, F., & Hodge, P. 1995, ApJ, 446, 616
Waller, W. H. 1991, ApJ, 370, 144
Warin, S., Benayoun, J. J., & Viala, Y. P. 1996, A&A, 308, 535
Wiklind, T., & Henkel, C. 1989, A&A, 225, 1
Wild, W., Harris, A. I., Eckart, A., Genzel, R., Graf, U. U., Jackson, J. M., Russell, A. P. G., & Stutzki, J. 1992, A&A, 265, 447
Wilson, C. D. 1995, ApJ, 448, L97
Wilson, C. D., Howe, J. E., & Balogh, M. L. 1999, ApJ, 517, 174
Wilson, C. D., Scoville, N. Z., Freedman, W. L., Madore, B. F., & Sanders, D. B. 1988, ApJ, 333, 611
Wilson, C. D., Walker, C. E., & Thornley, M. D. 1997, ApJ, 483, 210
Wolfire, M. G., Tielens, A. G. G. M., & Hollenbach, D. J. 1990, ApJ, 358, 116
Young, J. S., Gallagher, J. S., & Hunter, D. A. 1984, ApJ, 276, 476
Young, J. S., & Scoville, N. Z. 1991, ARA&A, 29, 581